nature physics

ARTICLES

PUBLISHED ONLINE: 20 JULY 2009 | DOI: 10.1038/NPHYS1338

Mimicking celestial mechanics in metamaterials

Dentcho A. Genov[1,2], Shuang Zhang[1] and Xiang Zhang[1,3]*

Einstein's general theory of relativity establishes equality between matter–energy density and the curvature of spacetime. As a result, light and matter follow natural paths in the inherent spacetime and may experience bending and trapping in a specific region of space. So far, the interaction of light and matter with curved spacetime has been predominantly studied theoretically and through astronomical observations. Here, we propose to link the newly emerged field of artificial optical materials to that of celestial mechanics, thus opening the way to investigate light phenomena reminiscent of orbital motion, strange attractors and chaos, in a controlled laboratory environment. The optical–mechanical analogy enables direct studies of critical light/matter behaviour around massive celestial bodies and, on the other hand, points towards the design of novel optical cavities and photon traps for application in microscopic devices and lasers systems.

The possibility to precisely control the flow of light by designing the microscopic response of an artificial optical material has attracted great interest in the field of optics. This ongoing revolution, facilitated by the advances in nanotechnology, has enabled the manifestation of exciting effects such as negative refraction[1,2], electromagnetic invisibility devices[3–5] and microscopy with super-resolution[1,6]. The basis for some of these phenomena is the equivalence between light propagation in curved space and in a locally engineered optical material. Interestingly, a similar behaviour exists in the general theory of relativity, where the presence of matter–energy densities results in curved spacetime and complex motion of both matter and light[7,8]. In the classical interpretation, this fundamental behaviour is known as the optical–mechanical analogy and is revealed through the least-action principles in mechanics, determining how a particle moves in an arbitrary potential[9], and the Fermat principle in optics, describing the ray propagation in an inhomogeneous media[10].

The optical–mechanical analogy provides a rather useful link between the study of light propagation in inhomogeneous media and the motion of massive bodies or light in gravitational potentials. Surprisingly, a direct mapping of the celestial phenomena by observing photon motion in a controlled laboratory environment has not been studied so far in an actual experiment. Here, we propose realistic optical materials that facilitate periodic, quasi-periodic and chaotic light motion inherent to celestial objects subjected to complex gravitational fields. This dense optical media (DOM) could be readily achieved with the current technology, within the framework of artificial optical metamaterials. Furthermore, we introduce a new class of specifically designed DOM in the form of continuous-index photon traps (CIPTs) that can serve as novel broadband, radiation-free and thus 'perfect' cavities. The dynamics of the electromagnetic energy confinement in the CIPTs is demonstrated through full-wave calculations in the linear and nonlinear regimes. Possible mechanisms for coupling light into the CIPTs and specific composite media are discussed.

Optical attractors and photonic black holes

One of the most fascinating predictions of the general theory of relativity is the bending of light that passes near massive celestial objects such as stars, nebulas or galaxies. This effect constituted one of the first pieces of evidence for the validity of Einstein's theory and provided a glimpse into the interesting predictions that were to follow. As shown, first by Schwarzschild and then by others, when the mass densities of celestial bodies reach a certain critical value (for example, through gravitation collapse), objects termed black holes form in space. Those entities fall under a more general class of dynamic systems, where a particular point, curve or manifold in space acts as an attractor of both matter and light. Such systems are of great interest for science not only in terms of the fundamental studies of light–matter interactions but also for possible applications in optical devices that control, slow and trap light. It is thus important to investigate the associated phenomena under controlled laboratory conditions.

In the general theory of relativity, a complex particle/photon motion is observed whenever the inherent spacetime is described by a metric g_{ij} that depends on the spatial coordinates $\mathbf{x} = \{x^1, x^2, x^3\}$ and universal time t. In such curved, non-static spacetimes, the propagation of matter and light rays follows the natural geodesic lines and is described by the Lagrangian

$$L = \frac{1}{2} g_{00}(\mathbf{x}, t)\dot{t}^2 - \frac{1}{2} g_{ij}(\mathbf{x}, t)\dot{x}^i \dot{x}^j \qquad (1)$$

where the derivatives are taken over an arbitrary affine parameter and natural units have been adopted. Here, we investigate the prospect to mimic the effect of curved spacetimes (equation (1)) on matter and light in the laboratory. To achieve this, we recognize that complex light motion is also observed in metamaterials described by inhomogeneous permittivities and permeabilities and could be related to light dynamics in curved space through the invariance of Maxwell's equations under coordinate transformations[4,5,11]. Metamaterials exhibiting complex electric and magnetic responses have been the focus of recent efforts to create negative-refractive-index media[1,2], electromagnetic cloaking[2–4] and as concentrators of light[12]. The above systems, however, suffer from high intrinsic loss and a narrow frequency range of operation and thus cannot be considered as prospective media to simulate light motion in a curved spacetime vacuum. Although the introduction of new metamaterials[13] may improve the overall performance, it is important to rely only on optical materials that are non-dissipative

[1]NSF Nanoscale Science and Engineering Center, University of California, Berkeley, California 94720, USA, [2]College of Engineering and Science, Louisiana Tech University, Ruston, Louisiana 71272, USA, [3]Material Sciences Division, Lawrence Berkeley National Laboratory, Berkeley, California 94720, USA.
*e-mail: xiang@berkeley.edu.

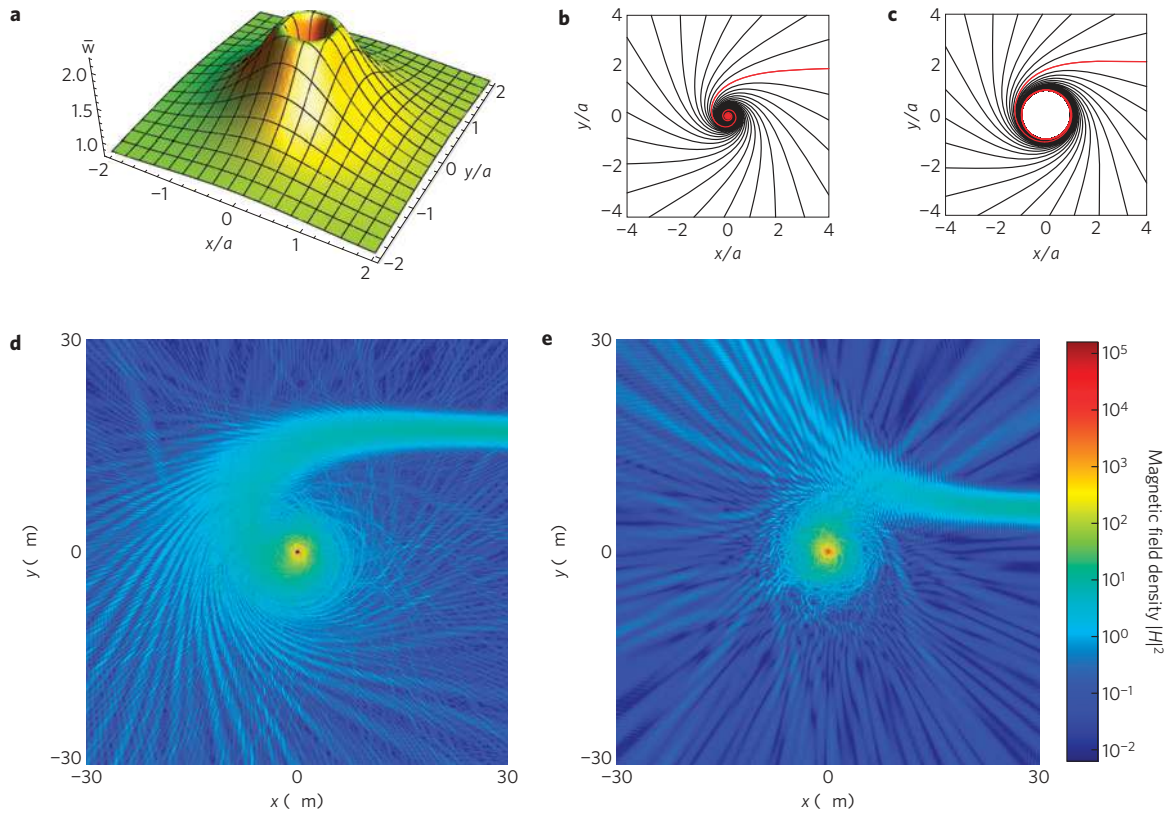

Figure 1 | Optical attractors and PBHs. a, Curved space corresponding to a PBH with $g_{00} = 1$ showing regions of spatial stretching and compression. Depending on their initial angular momentum (impact parameter s), the rays approaching the PBH will be deflected ($s > b$), attracted ($s < b$) or settle ($s = b$), on an unstable orbit. **b**,**c**, A set of such critical photon trajectories that fall into the singularity for $a = 0$ (**b**) or approach the unstable orbit at $a = 1$ (**c**) for an impact parameter $b = 2$. **d**,**e**, The FDFD calculation of the magnetic field density (the incident magnetic field is $|H_0| = 1$), corresponding to the critical trajectories with $b = 1.5a = 15\,\mu$m (**d**) and $b = 0.5a = 5\,\mu$m (**e**). In the calculations, very high energy densities are obtained close to the central attractor with the maximum value restricted only by the finite length scale that could be numerically investigated. The incident wavelength is $\lambda = 0.5\,\mu$m and the Gaussian beam width is $w = 4\lambda$.

and non-dispersive in general. For that, we consider a class of centrally symmetric metrics that can be written under coordinate transformation in an isotropic form (see the Methods section). For such curved spacetimes, light behaves in space similarly as in an optical media with an effective refraction index

$$n = (g/g_{00})^{1/2} \tag{2}$$

where $g = g_{11} = g_{22} = g_{33}$. The equivalence manifested in equation (2) is the basis for the studies of celestial phenomena in an actual table-top experiment. It enables the use of non-dissipative and non-dispersive dielectric materials. To demonstrate this, we propose a two-parameter family of isotropic centrally symmetric metrics $g = g_{00}((b/r)^2 + (1 - a/r)^2)$, where $r = |\mathbf{x}|$ is the radial coordinate and a and b are constants; constraint $\lim_{r\to\infty} g_{00} = 1$ is imposed to recover the flat space at large distances. The choice of this particular spacetime, which is schematically represented in Fig. 1a, has a number of important rationales. It exhibits a physical singularity at $r = 0$ and as shown below unstable photon orbits are supported at $r = a$, defining a photon sphere for the system[14]. These characteristics are reminiscent of a gravitational black hole in the general theory of relativity although the proposed metrics are not solutions to the Einstein field equations in a vacuum. Notwithstanding, here we refer to the considered system as a photonic black hole (PBH), or a spacetime where a particular point in space acts as an attractor of electromagnetic radiation.

Figure 1b,c demonstrates photon trajectories incident on the PBH with an impact parameter s, representing the minimal distance to the centre provided the photon is not deflected, that is equal to a critical value b. The Lagrangian formalism based on the curved spacetime equation (1) predicts that the impinging rays will inevitably reach their destiny at the central attractor/singularity (Fig. 1b), or asymptotically approach the photon sphere at $r = a$ (Fig. 1c). The spiral trajectories represent a critical point in the PBH phase space (see Supplementary Information) such that all photons approaching with impact factors less than or equal to the critical parameter b will never escape the system. Figure 1d,e shows full-wave simulations of Gaussian beams incident on a DOM with a refraction index profile described by equation (2) that maps the PBH space. The incident beams have propagation directions and initial positions set on the PBH critical trajectories (as in Fig. 1b,c), and the light is concurrently torn apart, with half the beams being scattered into infinity following hyperbolical paths, whereas the rest spirals into the central attractor. This ray behaviour is consistent with the expected ray trajectories in the original curved spacetime, but demonstrated in the equivalent DOM. In addition to the predicted ray behaviour, we observe electromagnetic energy density fluctuations (jets) leaving the system in radial directions (see Fig. 1e). This effect is due to the wave nature of light interaction with the inhomogeneous refraction index, and affects the electromagnetic rays that approach the PBH with impact factors slightly above the critical value. At the centre of the system, owing to the spacial singularity inherent to the PBH metrics, the effective refractive index approaches infinity. The singularly corresponds to an increasing stretching of space (see Fig. 1a), which acts as an effective 'potential well' attracting light. Concurrently, the

optical attractor can be considered as an effective 'cavity', decreasing both the group velocity and wavelength, which in turns gives rise to exceptionally high local energy densities.

Although the singularity in the refractive index profile of the ideal PBH is of fundamental interest for science, it is probably not feasible in practice. Such index profiles or the associated low group velocities have been discussed in the literature and specific systems have been suggested such as high-velocity vortex flow[15,16], microstructured nonlinear fibres[17], metamaterial waveguides[18], metal nanoparticles[19] and Bose–Einstein condensates[20]. Furthermore, close to the centre singularity, the ray picture fails and one cannot trust the predictions as per Fig. 1b,c. However, experimental observation of the main optical phenomena related to systems such as PBH or gravitational black holes does not necessitate exceptionally large refraction indices, or extremely low phase/group velocities. In fact, next we show that the underlying electromagnetic phenomena can be demonstrated using DOM in the form of simple binary metal–dielectric or pure dielectric composites.

Figure 2 shows finite refractive index profiles n mapped to that of a PBH, obtained by varying the volume fraction p of copper metal nanoparticles suspended in air (Fig. 2a) or air holes in a GaAs substrate (Fig. 2b). These composite materials can be nano-engineered through controlled deposition of metal particles in a dielectric host or growth of deep subwavelength in size air pockets in high-index materials. The electromagnetic phenomena associated with these realistic systems are shown in Fig. 2c,d, respectively. Despite the finite indices, the air–copper mixture can provide a complete picture of the far-field scattering profile inherent to a PBH (Fig. 2c), and photon 'trapping' into the unstable orbit (at the photon sphere) as well as critical behaviour at lower impact factors can be demonstrated in the air–GaAs composite (Fig. 2d). Specifically, at sufficiently large distances from the PBH ($r \gg \max(a,b)$), the light rays are deflected by an angle $\phi = -2a/s$ (Fig. 2c) that has the same dependence on the impact parameter s as that of the Einstein angle for gravitational lensing, but with reversed sign[8]. This results in a diverging energy flux at large distances with maximum field intensity observed at $y_m = (8a|x|)^{1/2}$. As metals are highly dispersive, the air–copper system will have a narrow operational bandwidth around the plasma resonance wavelength $\lambda_p = 0.27\,\mu$m, and the incident light will suffer energy loss, which although much lower compared with current metamaterials is still considerable (the imaginary part of the effective index is shown in Fig. 2a). To overcome these obstacles, one can instead design a pure dielectric media based on air–GaAs composites. Owing to the larger refractive index of the semiconductor ($n_{max} = n_{GaAs} = 3.25$; ref. 21), for this system, it is even possible to follow the light propagation in the region of space below the photon sphere with significantly reduced intrinsic losses and for a wide range of frequencies (below the GaAs bandgap). This is shown in Fig. 2d, where four Gaussian beams are sent into the system with initial angular moments and positions centred on critical trajectories. All beams asymptotically approach the photon sphere where they are ripped apart, with half the energy being scattered into the far-field, and the rest collapses towards the centre. The electromagnetic density fluctuations or 'jets' of energy leaving the photon sphere are clearly seen. To guarantee that this new phenomenon is not due to the truncated region below the photon sphere, an index-matched absorption core is used. The absorption core has the role of the central attractor and assures that all scattering and wave phenomena are properly represented by the DOM.

Overall, the DOM as per Fig. 2c provides the means to study electromagnetic wave interactions with critical points in spacetime (in particular the photon sphere) in a relatively simple table-top experiment. Such critical (saddle) points have an important role in establishing the overall system dynamics and can serve as a source of instability and chaos. The full range of DOM's applications including concentrating and storing electromagnetic energy are discussed next.

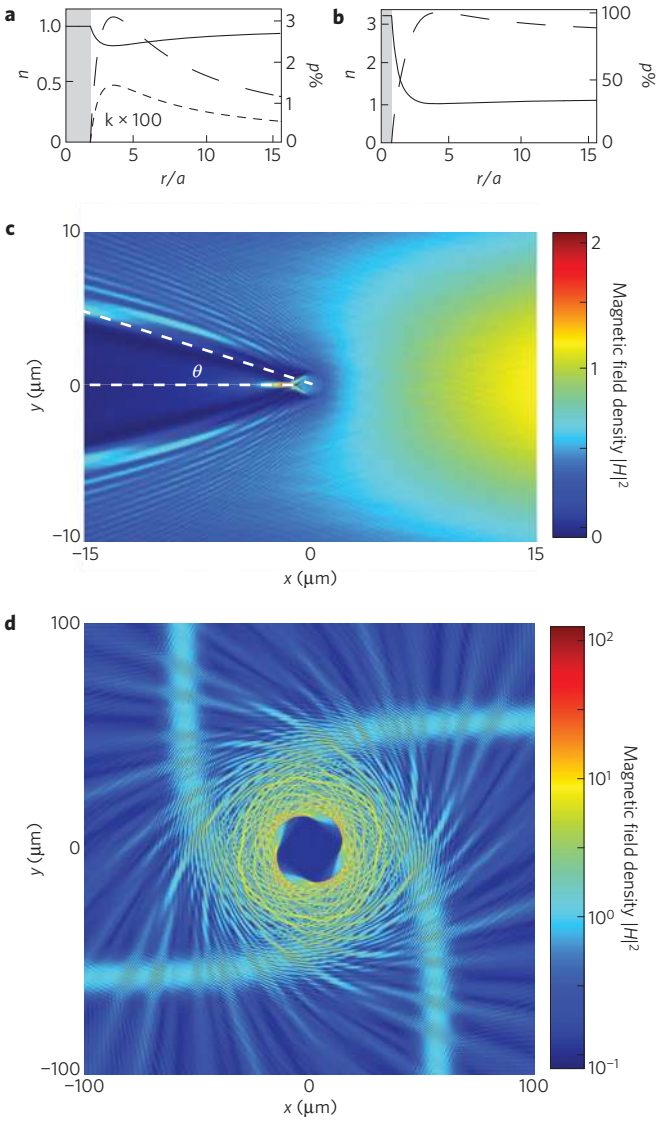

Figure 2 | Mimicking the PBH electromagnetic phenomenon in the laboratory. a–d, Mixtures of low-concentration copper metal nanoparticles in air (**a**) and air–GaAs composite media (**b**) can be used to provide the far-field scattering of the PBH with a scattering angle $\theta = \tan^{-1}(y_m/|x|)$ (**c**) and critical behaviour in the vicinity of the photon sphere (**d**), respectively. The effective refractive indices of the composites are presented with solid and short-dashed lines for the real and imaginary parts, respectively, and long-dashed lines are used for the metal/air volume fractions. The shaded areas in **a** and **b** represent the region of space where the refraction indices are truncated. In the FDFD calculations, we have set **c**, $a = 0.25\,\mu$m, $b = 1.5a$ and **d**, $a = 30\,\mu$m, $b = 50\,\mu$m. The incident wavelengths and beam widths are $\lambda = 0.24\,\mu$m ($w = 20\lambda$) and $\lambda = 1.55\,\mu$m ($w = 8\lambda$), respectively. For the air–GaAs composite, the absorption coefficient is fixed at 5 cm^{-1} (the intrinsic semiconductor absorption for frequency below the bandgap)[21] everywhere in space except within the truncation region where it is increased to 100 cm^{-1} to simulate the energy sink represented by the central attractor.

Photon traps, orbital motion and high-*Q*-factor cavities

The equivalence between light ray motion around massive celestial objects and in an artificially engineered optical medium has strong implications as the general formalism, represented by the

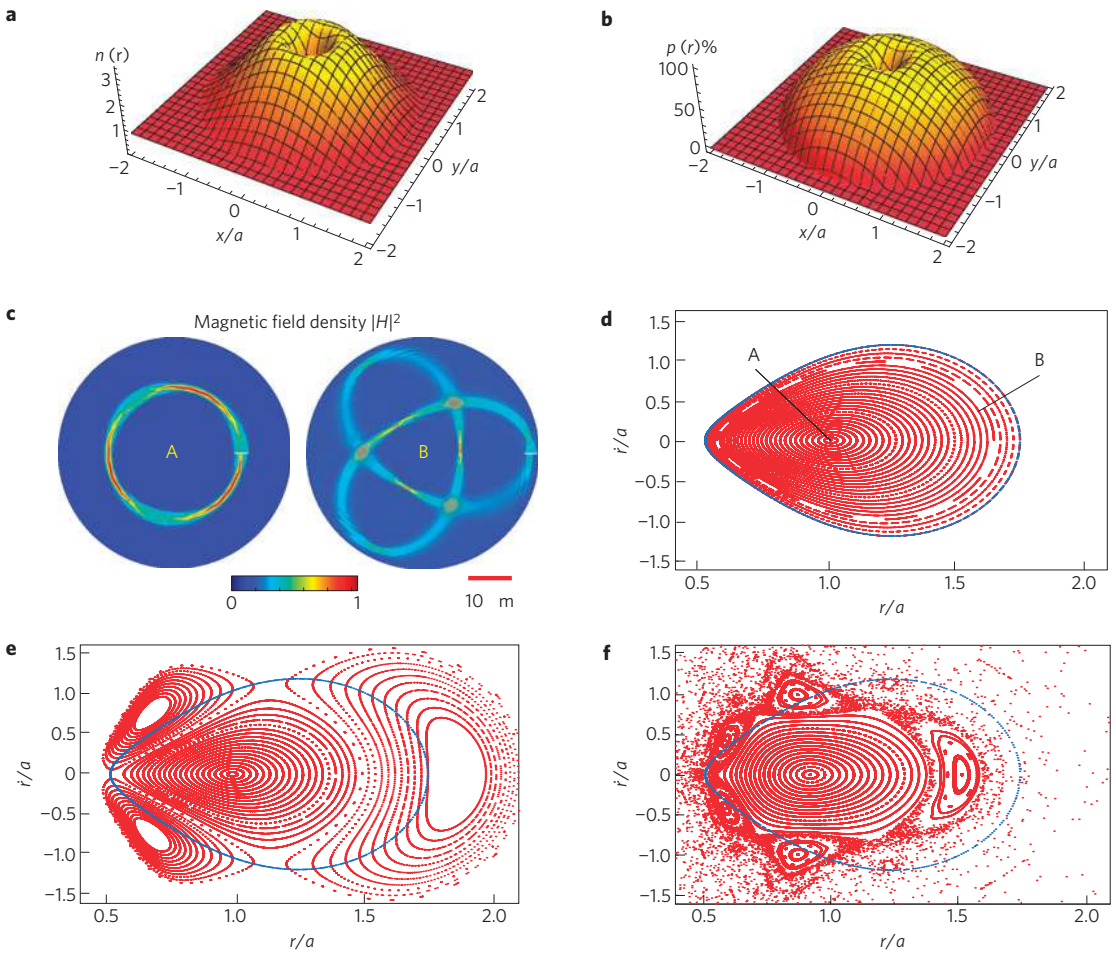

Figure 3 | CIPTs based on air–GaInAsP composite media. a,**b** Refractive index profile (**a**) and volume fraction (**b**) of the GaInAsP. **c**, FDFD simulations of bound and stable light propagation in the form of A, a circular orbit with period 2π and B, a 'Rosetta' type of orbit with period 4π. In the calculations, a linear source with width $w = 6\lambda$ and wavelength $\lambda = 1.55\,\mu$m is used. **d**–**f**, Poincaŕe maps (P_T) corresponding to all possible photon trajectories for linear (**d**) and nonlinear (**e**,**f**) refractive indices. In the linear case, the photon motion follows stable periodic and quasi-periodic trajectories for all initial conditions. With the introduction of nonlinearity, the stability of the system is disturbed with some trajectories passing through the cavity boundaries and leaving the system. **f**, For above-critical values of the nonlinear index $\Delta n_{NL}/n_{max} = 0.2$, chaotic behaviour is observed similarly to the three-body problem in celestial mechanics. In generating the Poincaŕe maps, the scale-invariant parameters r/a and $\dot{r}/a$ are sampled at times $t_m = 2\pi m/\omega_{NL}$ that are an integer number m of the nonlinear period (or T-period map), and the derivative is taken with respect to the azimuth angle φ.

Lagrangian equation (1), also describes restricted motion of matter in potential fields. Namely, under certain conditions the dynamics of matter in complex gravitational potentials can be replicated by the propagation of light in DOM. Here, we introduce an interesting prospective, with significant practical importance, which is to mimic planetary motion in the form of a stable and confined photon trajectory.

According to Bertrand's theorem[22], a general particle orbit in classical mechanics is stable and closed under any perturbations only in two types of central potential: Kepler's problem $U = -m/r < 0$ and the harmonic oscillator $U = mr^2 \geq 0$, where m is the mass. The theorem, however, demands further restrictions in optics where it can be shown that Kepler's potential no longer supports stable and closed circular or elliptical orbits for photons. This conclusion follows from the kinematic analogy[10], which casts the dynamic eikonal (ray) equation in a classical mechanical form with effective potential and kinetic energies $U = -K = -n^2/2$ directly related to the refraction index. Thus, in contrast to a particle that may have positive or negative total energy $U + K$, photons are equivalent to 'zero' energy states, which also follows from the null geodetic condition $L \to 0$, or the finite speed of light. As a consequence, only parabolic solutions are supported in this particular case.

Although Bertrand's theorem states that bound and exponentially stable photon orbits that are closed under any perturbations may not exist in centrally symmetric media, it does not preclude bound and stable motion that is not necessarily closed under perturbations; that is, the perturbed trajectory may cover a finite volume of space. Here, we propose a universal family of optical systems that exhibit those characteristics. The effective refractive indices can be directly obtained from the stability condition of the Lagrangian (1) resulting in

$$n(r) = \frac{A}{r}\exp\left(\int \frac{\chi(r)}{r}\,\mathrm{d}r\right) \qquad (3)$$

where $\chi(r)$ is an arbitrary monotonously decreasing function and A is a constant (see Supplementary Information). The above family of refractive indices, which we refer to as CIPTs, support stable circular and complex ray motion.

To illustrate this statement, we consider the most simple case where $\mathrm{d}\chi/\mathrm{d}r = -\kappa/a(\kappa \geq 0)$. The corresponding refraction indices are then obtained from equation (3) and can be written as $n = n_s(a/r)^{1-\kappa}\mathrm{e}^{-\kappa r/a}$, where a is the radius of the desired circular orbit and n_s is an arbitrary scaling factor. Furthermore,

we choose the $\kappa = 2$ case, and design the CIPT as an air–GaInAsP composite. This specific material system has been selected to provide operation at the infrared spectral range, using the high refractive index of the GaInAsP at low absorption, which for frequencies below the bandgap ($\hbar\omega_g = 1.2$ eV) is less than 1 cm^{-1} (ref. 21). The actual index and air volume fractions are shown in Fig. 3a,b. Full-wave simulations of two light trajectories for linear sources positioned at $r_{in} = a$ and $r_{in} = 1.62a$ are shown in Fig. 3c. According to the CIPT phase space shown in Fig. 3d, all ray trajectories are confined in space and the photon trapping is achieved without involving index discontinuities at the boundaries between different media. These bulk type of cavities where the trapped light satisfies the Lyapunov stability condition, constitutes a substantial improvement compared with the conventional gradient refraction index waveguides, and to the best of our knowledge, has not been studied in the literature. The CIPTs may provide new directions for the development of optical devices and high-Q-factor cavities for electromagnetic energy storage with minimal radiation losses. Specifically, coupling CIPTs with a light source, such as a quantum dot, could result in enhanced spontaneous emission, strong atom–photon coupling (cavity quantum electrodynamics), Raman lasing or enhanced high-order optical nonlinearities. These phenomena are due to the decreased photon decay rate, which for CIPTs is $\Gamma = \Gamma_i + \Gamma_r \approx \Gamma_i = \omega \mathrm{Im}n/\mathrm{Re}n$, where i and r stand for intrinsic dissipation and radiation loss, respectively. The CIPT quality factor $Q = \omega/\Gamma$ is thus limited only by the intrinsic loss and can be on par or larger than those of photonic crystals[23] and disc microcavities[24]. In the case of the air–GaInAsP composite, the quality factor can be as high as 10^6 when taking into account the actual material absorption in the semiconductor[21]. Furthermore, the Laypunov's stability of the photon trajectories implies that finite index variations due to fabrication imperfections will not lead to photon loss from the CIPT; the photons simply hop to another close-by bound trajectory (see Fig. 3d). This is another advantage of CIPTs in respect to conventional cavities and waveguides where light scattering at surface or volume imperfections can lead to photons escaping from the system.

Nonlinearity and chaos

The onset of chaos in dynamic systems is one of the most fascinating problems in science and is observed in areas as diverse as molecular motion[25], population dynamics[26] and optics[27]. In particular, a planet around a star can undergo chaotic motion if a perturbation, such as another large planet, is present. However, owing to the large spatial distances between the celestial bodies, and the long periods involved in the study of their dynamics, the direct observation of chaotic planetary motion has been a challenge[28]. The use of the optical–mechanical analogy may enable such studies to be accomplished in the laboratory. Furthermore, in the case of the CIPTs, where trapping of light occurs with unprecedented lifetimes, the onset of chaos could enable access to those closed ray trajectories from the far-field. This is directly addressed by involving the analogy with the celestial mechanics where a third-body perturbation can be modelled as a periodic nonlinear refraction index modulation; $n(r,t) = n_{\mathrm{CIPT}}(r) + \Delta n_{\mathrm{NL}} \sin^2(\omega_{\mathrm{NL}} t)$ introduced by an external electrical or electromagnetic source.

The Poincaŕe maps of the photon motion under these settings are shown in Fig. 3e,f. In contrast to the non-perturbed linear case (Fig. 3d), where all photon trajectories are closed and determined by the first integral of the system, the introduction of nonlinear harmonic variations brings a fundamentally different behaviour. For $\Delta n_{\mathrm{NL}}/n_{\max} = 0.05$ (Fig. 3e), and period of the modulations $T = 2\pi/\omega_{\mathrm{NL}} = 6c/a$, we observe substantial expansion of the original phase space, the boundary of which is marked with a blue line. The original invariant curves have broken up into four separate domains. As a result, photons may pass at distances $r > r_{\max} = 1.74a$, where the CIPT refractive index truncates to unity. Those light rays will escape on reaching the outer boundary or concurrently, external light could be coupled into the otherwise perfect cavity (in the linear sense). This is accomplished if the nonlinearity is switched off for times $t < a/c$, leading to a fraction of the impinging light being trapped inside the system. Similar behaviour could be observed even for moderate nonlinearities $\Delta n_{\mathrm{NL}}/n_{\max} < 0.01$, in which case a smaller fraction of the CIPT phase space could be accessed from the far-field. The considered levels of nonlinearities are available with semiconductor materials such as GaInAsP at frequencies close to the band edge[29], liquid crystals[30] or multiple quantum wells[31]. Furthermore, the strong modification of the phase space and the breaking up of the original invariant curves into islands is prerequisite behaviour for the onset of chaos. Indeed, at very high nonlinearities, an ever-increasing breaking-up of the regular motion reaches a point where the phase space acquires strongly chaotic characteristics, as shown in Fig. 3f. Such complex motion is directly related to the three-body problem in celestial mechanics and underlines the optical–mechanical analogy and its broad applicability.

Methods

The invariance of Maxwell's equations under coordinate transformations brings the equivalence between curved spacetime and local optical response through spatially dependent permeability and permittivity tensors. Specifically, light motion in the spacetime metric with the line element

$$\mathrm{d}s^2 = g_{00}\mathrm{d}t^2 - g_{ii}\,\mathrm{d}x^i\mathrm{d}x^i \tag{4}$$

is equivalent to that in an effective media with local permeability and permittivity tensors given as

$$\mu_{ij} = \varepsilon_{ij} = \delta_{ij}\frac{h_1 h_2 h_3}{h_i\sqrt{g_{00}}}$$

where $h_i = \sqrt{g_{ii}}$ are the Lame coefficients of the transformation between the curved metric equation (4) and flat space[4,11], and the factor $\sqrt{g_{00}}$ is the redshift/blueshift correction due to time dilation. To eliminate the need for such complex behaviour, we concentrate on a class of centrally symmetric metrics that can be written under coordinate transformation in an isotropic form $\mathrm{d}s^2 = g_{00}(r,t)\,\mathrm{d}t^2 - g(r,t)\mathrm{d}\mathbf{x}^2$. Thus, the effective refraction index n is also isotropic and can be achieved with dielectric materials (see Supplementary Informations for details).

To schematically represent the PBH metrics (see Fig. 1a), we consider only lateral space stretching or compression by means of a normalized Euclidean coordinate $\tilde{w} = w(r)/r$ as per $\mathrm{d}s^2 = \mathrm{d}t^2 - g_{rr}(r)\,\mathrm{d}r^2 = \mathrm{d}t^2 - \mathrm{d}w^2$, where $g_{rr} = n^2$. In Fig. 1b,c, we also show photon motion corresponding to the first integral of the system (equation (1)), which is a family of exponential spiral trajectories $r = a \times (1 - \mathrm{e}^{(\varphi_0 - \varphi)a/b})^{-1}$, where φ_0 is the angle of approach at infinity.

The DOM effective indices and volume fractions of the inclusions (Figs 2 and 3) are estimated from the effective-medium approximation[32] and Maxwell–Garnett theory[33] for the dielectric–dialectic and metal–dielectric composites, respectively. Commercial software FEMLAB has been used for the electromagnetic finite-difference frequency domain (FDFD) calculations throughout the paper.

Received 16 May 2008; accepted 12 June 2009; published online 20 July 2009

References

1. Pendry, J. B. Negative refraction makes a perfect lens. *Phys. Rev. Lett.* **85,** 3966–3969 (2000).
2. Shelby, R. A., Smith, D. R. & Schultz, S. Experimental verification of a negative index of refraction. *Science* **292,** 77–79 (2001).
3. Leonhardt, U. Optical conformal mapping. *Science* **312,** 1777–1780 (2006).
4. Pendry, J. B., Schurig, D. & Smith, D. R. Controlling electromagnetic fields. *Science* **312,** 1780–1782 (2006).
5. Leonhardt, U. & Philbin, T.G. General relativity in electrical engineering. *New J. Phys.* **8,** 247–265 (2006).
6. Fang, N., Lee, H., Sun, C. & Zhang, X. Sub-diffraction-limited optical imaging with a silver superlens. *Science* **308,** 534–537 (2005).
7. Kox, A. J. *et al.* (eds) *The Collected Papers of Albert Einstein* Vol. 6 (Princeton Univ. Press, 1997).
8. Einstein, A. Lens-like action of a star by the deviation of light in the gravitational field. *Science* **84,** 506–507 (1936).

9. de Maupertuis, P. L. M. Accord de différentes lois de la nature qui avaient jusqu'ici paru incompatibles. *Mém. As. Sc. Paris* 417–427 (1744).
10. Evans, J. The ray form of Newton's law of motion. *Am. J. Phys.* **61,** 347–350 (1993).
11. Plebanski, J. Electromagnetic waves in gravitational fields. *Phys. Rev.* **118,** 1396–1408 (1960).
12. Kildishev, A. V. & Shalaev, V. M. Engineering space for light via transformation optics. *Opt. Lett.* **33,** 43–45 (2008).
13. Valentine, J. *et al.* Three dimensional optical metamaterial exhibiting negative refractive index. *Nature* **455,** 376–379 (2008).
14. Shapiro, S. L. & Teukolsky, S. A. *White Dwarfs, and Neutron Stars: The Physics of Compact Objects* (Wiley, 1983).
15. Leonhardt, U. & Piwnicki, P. Relativistic effects of light in moving media with extremely low group velocity. *Phys. Rev. Lett.* **84,** 822–825 (2000).
16. Visser, M. Comment on "Relativistic effects of light in moving media with extremely low group velocity". *Phys. Rev. Lett.* **85,** 5252–5252 (2000).
17. Philbin, T. G. *et al.* Fiber-optical analog of the event horizon. *Science* **319,** 1367–1370 (2008).
18. Tsakmakidis, K. L., Boardman, A. D. & Hess, O. Can light be stopped in realistic metamaterials? *Nature* **455,** E11–E12 (2008).
19. Bashevoy, M., Fedotov, V. & Zheludev, N. Optical whirlpool on an absorbing metallic nanoparticle. *Opt. Express* **13,** 8372–8379 (2005).
20. Hau, L. V. *et al.* Light speed reduction to 17 m s^{-1} in an ultracold atomic gas. *Nature* **397,** 594–598 (1999).
21. Levinstein, M., Rumyantsev, S. & Shur, M. (eds) *Handbook Series on Semiconductor Parameters* Vol. 1, 2 (World Scientific, 1996, 1999).
22. Bertrand, J. Mecanique analytique. *C. R. Acad. Sci.* **77,** 849–853 (1873).
23. Painter, O. *et al.* Two-dimensional photonic band-gap defect mode laser. *Science* **284,** 1819–1821 (1999).
24. Armani, D. K. *et al.* Ultra-high-*Q* toroid microcavity on a chip. *Nature* **421,** 925–928 (2003).
25. Wu, G. *Nonlinearity and Chaos in Molecular Vibrations* (Elsevier, 2005).
26. Costantino, R. F., Desharnais, R. A., Cushing, J. M. & Dennis, B. Chaotic dynamics in an insect population. *Science* **275,** 389–391 (1997).
27. Zheludev, N. I. Polarization instability and multistability in nonlinear optics. *Usp. Fiz. Nauk* **157,** 683–717 (1989).
28. Malhotra, R., Holman, M. & Ito, T. Chaos and stability of the solar system. *Proc. Natl Acad. Sci. USA* **8,** 12342 (2001).
29. Islam, M. N., Ippen, E. P., Burkhardt, E. G. & Bridges, T. J. Picosecond nonlinear absorption and four-wave mixing in GaInAsP. *Appl. Phys. Lett.* **47,** 1042–1044 (1985).
30. Lucchetti, L. *et al.* Colossal optical nonlinearity in dye doped liquid crystals. *Opt. Commun.* **233,** 417–424 (2004).
31. Brzozowski, L. *et al.* Direct measurements of large near-band edge nonlinear index change from 1.48 to 1.55 μm in InGaAs/InAlGaAs multiquantum wells. *Appl. Phys. Lett.* **82,** 4429–4431 (2003).
32. Bruggeman, D. A. G. Berechnung verschiedener physikalischer Konstanten von heterogenen Substanzen. *Ann. Phys. (Leipzg)* **24,** 636–679 (1935).
33. Maxwell-Garnett, J. C. Colours in metal glasses and in metallic films. *Phil. Trans. R. Soc. Lond.* **203,** 385–420 (1904).

Acknowledgements

This work has been supported by US Army Research Office ARO MURI program 50432–PH-MUR, the NSF Nano-scale Science and Engineering Center (NSEC) under Grant No. CMMI-0751621 and Louisiana Board of Regents under contract number LEQSF (2007-12)-ENH-PKSFI-PRS-01. We would also like to thank G. Bartal and D. Pile for important discussions and assistance.

Author contributions

D.A.G. conceived and implemented the theory and numerical simulations, designed the DOM and CIPT media and prepared the manuscript; S.Z. and X.Z. contributed extensively in the data analyses and conceptualization, and edited the manuscript.

Additional information

Supplementary information accompanies this paper on www.nature.com/naturephysics. Reprints and permissions information is available online at http://npg.nature.com/reprintsandpermissions. Correspondence and requests for materials should be addressed to X.Z.